Opposing signatures of neural excitability and sensory input in initial cortical responses differentially predict intensity perception

Stephani, T.[1, 2]*, Hodapp, A. [1¶], Jamshidi Idaji, M. [1, 2, 4], Villringer, A.[1, 3, 5], Nikulin, V. V.[1, 6]*

[1] Department of Neurology, Max Planck Institute for Human Cognitive and Brain Sciences, Leipzig, Germany, 04103

[2] International Max Planck Research School NeuroCom, Leipzig, Germany, 04103

[3] Berlin School of Mind and Brain, Humboldt-Universität zu Berlin, Berlin, Germany, 10117

[4] Machine Learning Group, Technical University of Berlin, Berlin, Germany, 10587

[5] Clinic for Cognitive Neurology, University Hospital Leipzig, Leipzig, Germany, 04103

[6] Institute for Cognitive Neuroscience, National Research University Higher School of Economics, Moscow, Russian Federation, 101000

[¶] Now at Department of Psychology, University of Potsdam, Potsdam, Germany, 14476

* corresponding authors: T.S. (stephani@cbs.mpg.de); V.V.N. (nikulin@cbs.mpg.de)

Abstract

Perception of sensory information is determined by stimulus features (e.g., intensity) and instantaneous neural states (e.g., excitability). Commonly, it is assumed that both are reflected similarly in evoked brain potentials, that is, higher evoked activity leads to a stronger percept of a stimulus. We tested this assumption in a somatosensory discrimination task in humans, simultaneously assessing (i) single-trial excitatory post-synaptic currents inferred from short-latency somatosensory evoked potentials (SEP), (ii) pre-stimulus alpha oscillations (8-13 Hz), and (iii) peripheral nerve measures. Fluctuations of neural excitability shaped the perceived stimulus intensity already during the very first cortical response (at ~20 ms) yet demonstrating opposite neural signatures as compared to the effect of presented stimulus intensity. We reconcile this discrepancy via a common framework based on modulations of electro-chemical membrane gradients linking neural states and responses, which calls for reconsidering conventional interpretations of brain potential magnitudes in stimulus intensity encoding.

1 Introduction

Even for the very same stimulus, the brain´s response differs from moment to moment. This has been explained by ever-changing neural states (Arieli et al., 1996), specifically involving fluctuations of cortical excitability (Klimesch et al., 2007; Romei et al., 2008). In the human brain, a commonly hypothesized marker of cortical excitability is oscillatory activity in the alpha band (8-13 Hz), which can be measured with electro- and magnetoencephalography (EEG/MEG). This marker has been associated with modulations of a stimulus´ percept in various sensory domains including the visual (Busch et al., 2009; Iemi et al., 2017), auditory (Müller et al., 2013), and somatosensory domain (Baumgarten et al., 2016; Craddock et al., 2017; Forschack et al., 2020). According to the baseline sensory excitability model (BSEM; Samaha et al., 2020), higher alpha activity preceding a stimulus leads to a generally lower excitability level of the neural system, resulting in a lower detection rate of near-threshold stimuli but no changes in the discriminability of sensory stimuli. On a cellular level, such excitability modulations may be reflected in changes of membrane potentials (Castro-Alamancos, 2009), which may occur in an oscillatory manner (Lakatos et al., 2005) and shift the threshold for incoming sensory information to be processed further downstream in the neural system. This notion has further been supported by monkey studies showing that higher oscillatory activity within the alpha band is associated with a lower neural firing rate (Bollimunta et al., 2011; Haegens et al., 2011).

However, it remains unclear up to now whether the influence of instantaneous excitability on perceptual processes can be generalized to the intensity perception of stimuli *per se* (i.e., beyond the sensory threshold) – which would have far-reaching implications for a wide variety of studies in the field of perception. Moreover, if such modulation indeed occurs, the question remains: At which stage of the neural response cascade do instantaneous excitability changes begin to interact with the sensory input in order to shape the brain´s response in a behaviorally relevant way?

A unique opportunity to non-invasively measure instantaneous excitability changes of neurons involved in the first cortical response to sensory stimuli in humans is offered by the N20 component of the somatosensory evoked potential (SEP) as measured with EEG: The N20 component, a negative deflection after around 20 ms at centro-parietal electrode sites in response to median nerve stimulation, reflects excitatory post-synaptic potentials (EPSPs) of the first thalamo-cortical volley (Nicholson Peterson et al., 1995; Wikström et al., 1996; Bruyns-Haylett et al., 2017) which are generated in the anterior wall of the postcentral gyrus, Brodmann area 3b (Allison et al., 1991). When keeping the sensory input constant, the amplitude of this early part of the SEP thus represents a direct measure of the instantaneous excitability of a well-defined neuronal population in the primary somatosensory cortex. Notably, amplitude fluctuations of the N20 component have recently been found to relate to pre-stimulus alpha activity both at a given instance as well as through their long-term temporal dynamics, which suggests that both measures reflect a common modulating factor, that is cortical excitability (Stephani et al., 2020).

In the current study, we set out to examine the implications of instantaneous excitability fluctuations at initial cortical processing – as measured both by pre-stimulus alpha activity and N20 amplitudes – on the perceived intensity of somatosensory stimuli. We used a binary intensity rating task in which participants were to discriminate supra-threshold median nerve stimuli of two intensities in a continuous stimulation sequence (Fig. 1a). Our results show that both pre-stimulus alpha activity and N20 amplitudes are associated with a bias in the perceived intensity of somatosensory stimuli. Thus, instantaneous excitability fluctuations affect sensory brain responses already at earliest possible cortical processing with behaviorally relevant consequences. Counterintuitively, elevated neural excitability and stronger stimulus intensity resulted in reverse effects on short-latency SEP amplitudes, which in turn may offer further insights into the neural mechanisms of excitability regulation through resting membrane potentials.

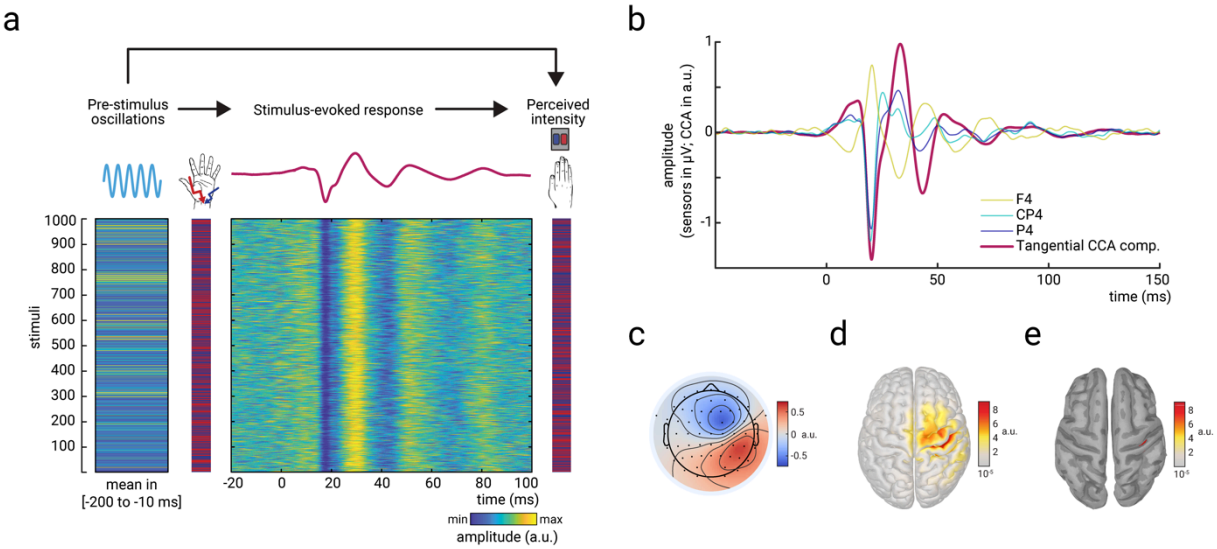

Fig. 1. Experimental paradigm and main electrophysiological measures. a) The relationships between pre-stimulus alpha oscillations, stimulus-evoked responses, and perceived intensity of somatosensory stimuli were examined in a continuous sequence of median nerve stimuli of two intensities with inter-stimulus intervals of ISI = 1513 ± 50 ms. After every stimulus, participants were to rate the perceived intensity as either "strong" or "weak" as fast as possible by button press. The raster plots represent the data of an exemplary subject with the rows corresponding to single trials. Displayed from left to right: Average pre-stimulus alpha amplitude, intensity of the presented stimuli (red=strong; blue=weak intensity), short-latency somatosensory evoked potentials (SEP), and the perceived intensity as reported by the participants (red=strong; blue=weak intensity). Alpha activity and the SEP were both retrieved from the *tangential CCA component* (displayed in panels b-e) and hence reflect activity of the same neuronal sources. b) Grand average of the SEP (N=32) in sensor space (electrodes F4, CP4, and P4) and for the *tangential CCA component* as derived from the single-trial extraction approach using Canonical Correlation Analysis (CCA). c) Activation pattern of the *tangential CCA component* displaying a tangential dipole contralateral to stimulation site over the central sulcus which is typical for the N20-P35 complex of the SEP. Averaged across participants (N=32). d) Neuronal sources (absolute values) underlying the activation pattern of the *tangential CCA component*, reconstructed using eLoreta inverse modeling. Averaged across participants (N=32). e) Same as d but applying an amplitude threshold of 95% in order to indicate the strongest generators of neural activity (displayed on a smoothed cortex surface).

2 Results

Behavioral results

Participants discriminated the weak and the strong stimuli with an average accuracy of acc_{mean} = 69.72% (*SD* = 7.94%; $CI_{95\%}$: [66.86%, 72.58%]), suggesting a moderate to high task difficulty. As confirmed by permutation tests, every individual participant performed better than chance level, all $p < .05$ (Bonferroni-corrected). The average discrimination sensitivity was d'_{mean} = 1.14 (*SD* = .46; $CI_{95\%}$: [0.98, 1.31]) and the average criterion c_{mean} = .01 (*SD* = .22; $CI_{95\%}$: [-.066, .094]), according to Signal Detection Theory (Green & Swets, 1966). Participants pressed the respective response button with an average reaction time of RT_{mean} = 642.42 ms (*SD* = 95.79 ms; $CI_{95\%}$: [607.89 ms, 676.96 ms]).

Extraction of single-trial somatosensory evoked potentials

Single-trial activity of the early SEP was extracted using a variant of Canonical Correlation Analysis (CCA; Fedele et al., 2013; Waterstraat et al., 2015), as previously reported for a similar paradigm examining the fluctuation of single-trial SEPs in response to stimuli with constant intensity (Stephani et al., 2020). This variant of CCA extracts a number of spatially distinct components based on a pattern matching between average SEP and single trials. Similar to Stephani et al. (2020), a prominent CCA component was identified in all subjects, that showed a clear peak at around 20 ms post-stimulus (Fig. 1b) and displayed the pattern of the typical N20 tangential dipole (Fig. 1c). Furthermore, neuronal sources of this CCA component were primarily located in the anterior wall of the post-central gyrus (Brodmann area 3b) in the primary somatosensory cortex (Fig. 1d & e). Single-trial SEPs from this – as is referred to in the following – *tangential CCA component* are displayed for an exemplary subject in Figure 1a.

Pre-stimulus alpha amplitude is associated with a bias in perceived stimulus intensity

To assess whether pre-stimulus neural states modulated the perception of upcoming somatosensory stimuli, we related oscillatory activity in the alpha band (8-13 Hz) before stimulus onset to the participants´ reports of perceived stimulus intensity. Alpha band activity was measured from the same neural sources as the SEP, applying the spatial filters of the tangential CCA component. Figure 2a shows the envelope of pre-stimulus alpha activity depending on the behavioral responses of the participants. Pre-stimulus alpha amplitude was higher when participants rated the stimulus to be weak rather than strong (regardless of the actual stimulus intensity). This observation was further quantified with Signal Detection Theory (SDT; Green & Swets, 1966) in order to differentiate the ability to discriminate stimulus intensities, as measured by *sensitivity d'*, from a response bias towards either strong or weak perceived intensity, as measured by *criterion c*. In correspondence with a recent study in the visual domain (Iemi et al., 2017), these SDT-derived parameters were statistically compared between the 20% of trials with the lowest and the 20% of trials with the highest pre-stimulus alpha amplitudes (as averaged in a time window from 200 to 10 ms before the stimulus onset; Fig. 2b). A paired-sample *t*-test confirmed a difference regarding *criterion c*, $t(31) = -2.777$, $p = .009$, *Cohen´s d* = -.491, with average criterions of $c_{\text{lowest20\%}} = -.009$ and $c_{\text{highest20\%}} = .060$ ($CI_{95\%}$ of difference: [-.119, -.018]). No difference was found for *sensitivity d'*, $t(31) = -1.425$, $p = .164$, *Cohen´s d* = -.252, with average sensitivities $d'_{\text{lowest20\%}} = 1.058$ and $d'_{\text{highest20\%}} = 1.142$ ($CI_{95\%}$ of difference: [-.204, .036]). Thus, higher pre-stimulus alpha amplitude was associated with a higher threshold to rate the stimulus as "strong", corresponding to a bias to generally report lower stimulus intensities, whereas the discriminability between the stimulus categories appeared unaffected.

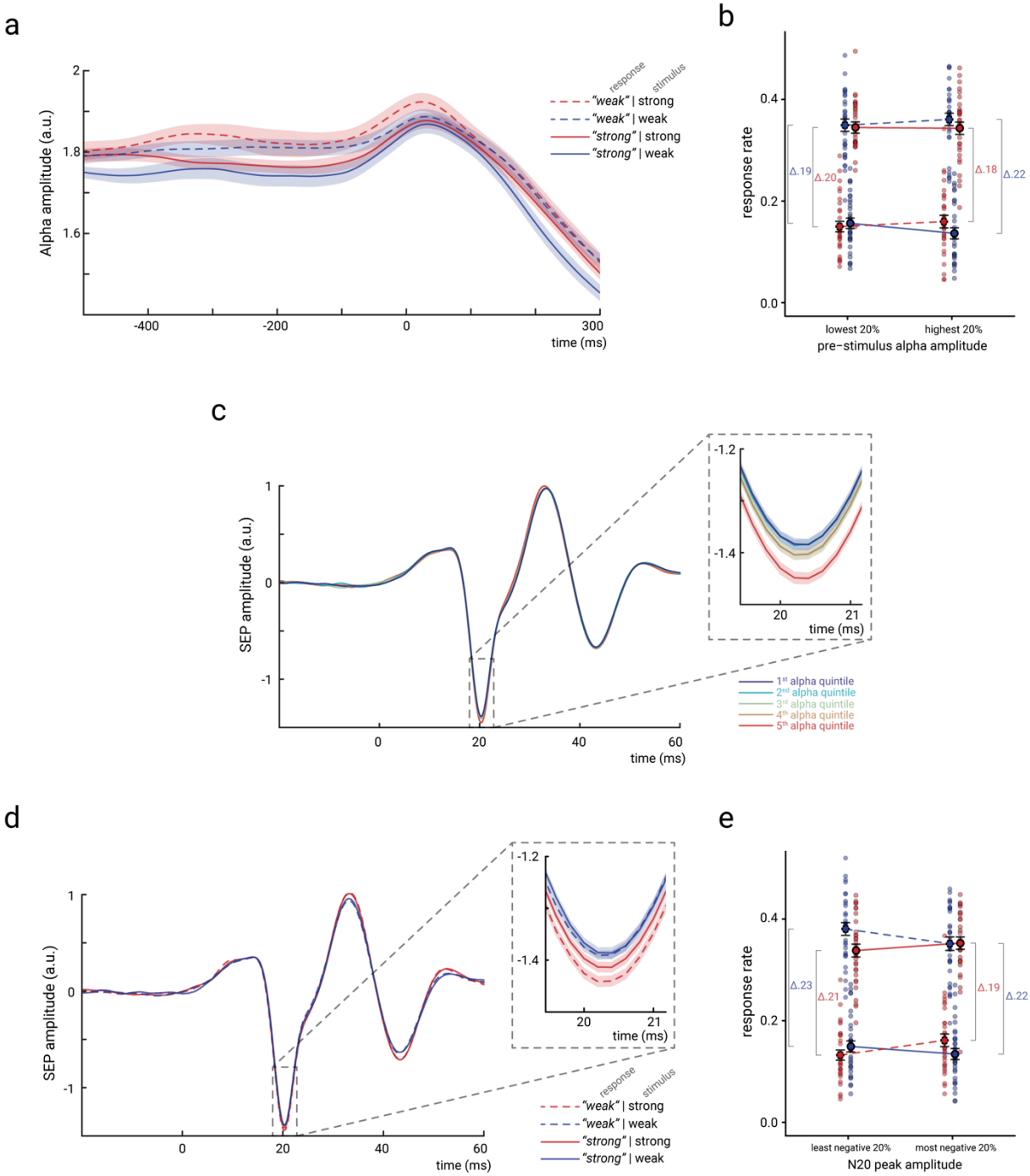

Fig. 2. Bi-variate relationships between pre-stimulus alpha amplitude, N20 peak amplitude, and perceived stimulus intensity. a) Time course of the amplitude of pre-stimulus alpha band activity (8-13 Hz) displayed by behavioral response categories. Note that for statistical analyses, pre-stimulus epochs were cut at -5 ms relative to stimulus onset *before* filtering the data in the alpha band (8-13 Hz), in order to prevent contamination of the pre-stimulus window by stimulus-related activity. b) Rate of response categories for the lowest and highest alpha amplitude quintiles (as measured between -200 and -10 ms). Δ indicates the difference in response rates within each stimulus category. c) SEP (tangential CCA component) sorted with respect to pre-stimulus alpha amplitude quintiles. Alpha quintiles were sorted in ascending order (i.e., 1st quintile = lowest alpha amplitude). d) SEP (tangential CCA component) sorted according to behavioral response categories. e) Rate of response categories for the least and most negative N20 peak amplitude quintiles. Δ indicates the difference in response rates within each stimulus category. All panels show the grand average across all participants (N=32). Shaded areas in panels a, c, and d, as well as error bars in panels b and e correspond to the standard errors of the mean based on the within-subject variances (Morey, 2008). Transparent points in panels b and e reflect data of individual participants.

Pre-stimulus alpha amplitude is associated with single-trial N20 amplitudes

Following the hypothesis that both pre-stimulus alpha band activity and the N20 component of the SEP reflect changes in instantaneous cortical excitability, a covariation of these two measures should be expected (Stephani et al., 2020). Indeed, higher pre-stimulus alpha amplitudes were associated with larger (i.e., more negative) N20 peak amplitudes (Fig. 2c), as statistically tested with a random-slope linear-mixed-effects model, β_{fixed} = -.023, $t(32.17)$ = -2.969, p = .006 ($CI_{95\%}$ of β_{fixed}: [-0.040, -0.007]). Notably, the direction of this effect may appear counter-intuitive at first sight but can be explained by the physiological basis of EEG generation, which offers important insights into the functional link between pre-stimulus alpha activity and SEP (see Discussion section *Opposing signatures of presented stimulus intensity and excitability in the early SEP*).

Single-trial N20 amplitudes are associated with a bias in perceived stimulus intensity

Given the relationships of pre-stimulus alpha activity with perceived stimulus intensity and N20 peak amplitudes, we tested whether the latter also related to the SDT parameters of the behavioral performance. In parallel to the analyses of the effect of pre-stimulus alpha activity, *sensitivity d'* and *criterion c* were statistically compared between the 20% of trials with the most negative and the 20% of trials with the least negative N20 peak amplitudes. Again, a difference emerged for *criterion c*, $t(31)$ = 2.306, p = .028, *Cohen's d* = .408, with average criterions of $c_{\text{most neg.20\%}}$ = .055 and $c_{\text{least neg.20\%}}$ = .000 ($CI_{95\%}$ of difference: [.006, .104]), as assessed with a paired-sample *t*-test. No effect emerged for *sensitivity d'*, $t(31)$ = -1.747, p = .091, *Cohen's d* = -.309, with $d'_{\text{least neg.20\%}}$ = 1.213 and $d'_{\text{most neg.20\%}}$ = 1.142 ($CI_{95\%}$ of difference: [-.154, .012]). Thus, c*riterion c* was lower for less negative than for more negative N20 peak amplitudes. This response bias becomes evident from the differences in the response rates (Δ) within each stimulus category in Figure 2e: Although Δs decrease from the *least negative 20%* bin to the *most negative 20%* bin for both

strong and weak stimuli, the decrease is larger in strong than in weak stimuli. Thus, participants were overall more likely to rate a stimulus as "strong" rather than "weak" when N20 amplitudes were smaller, when taking into account the stimulus´ actual intensity, as also reflected in Figure 2d. This effect was further corroborated by comprehensive structural equation modelling on a single-trial level as described in the following section.

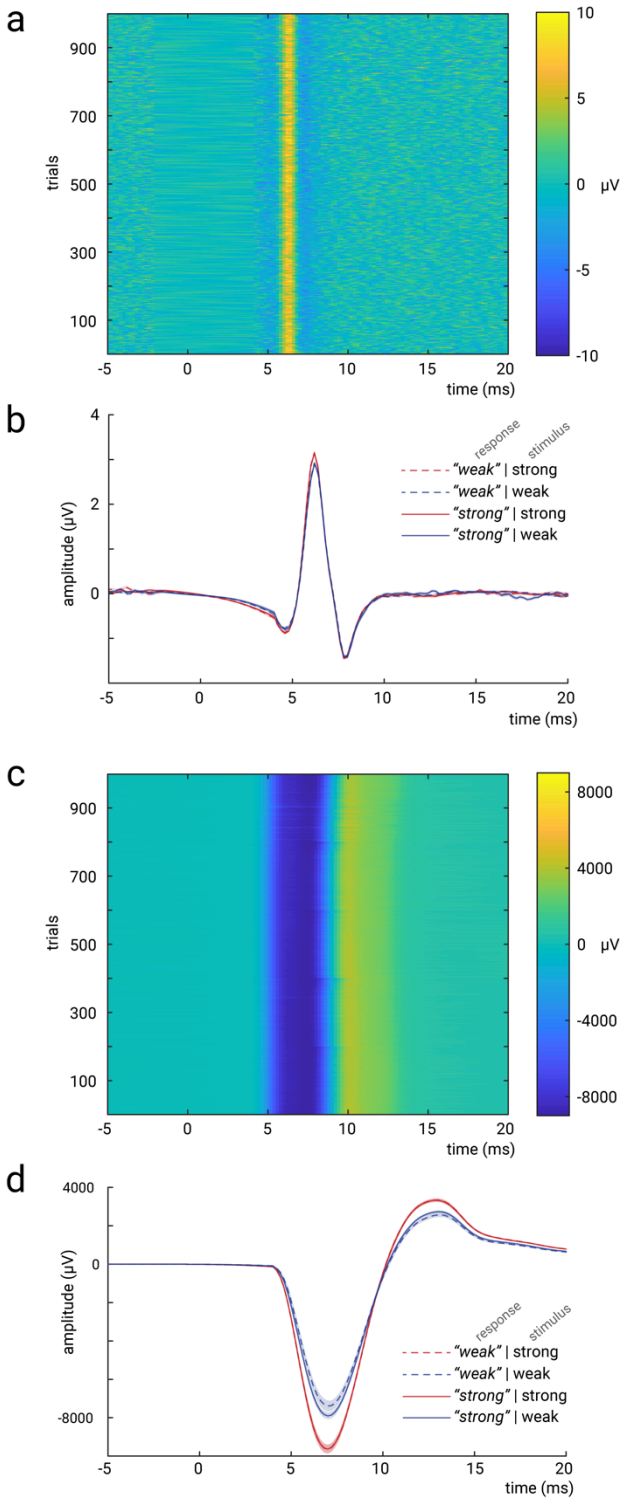

Fig. 3. Measures to control for peripheral nerve variability. a) Single trials of the *compound nerve action potential (CNAP)* in response to the median nerve stimuli, measured at the inner side of the ipsilateral upper arm (shown for an exemplary subject). b) Grand average across participants (N=32) of the CNAP, displayed by stimulus and response types. c) Single trials of the *compound muscle action potential (CMAP)*, measured at the M. abductor pollicis brevis (shown for an exemplary subject). d) Grand average across participants (N=32) of the CMAP, displayed by stimulus and response types. Shaded areas in panels b and d correspond to the standard errors of the mean based on the within-subject variances (Morey, 2008).

Structural equation modeling of effect paths

Importantly, Figures 2d & 2e also suggest that N20 amplitudes were generally larger (i.e., more negative) for higher stimulus intensities – thus showing an effect of opposite direction on N20 amplitudes than instantaneous cortical excitability. In order to disentangle these effects of excitability and stimulus intensity, we examined their respective contributions in a two-level structural equation model, with *stimulus intensity*, *pre-stimulus alpha amplitude*, and *N20 peak amplitude* as predictors of *perceived stimulus intensity* on level 1 (within subjects), and random intercepts as well as their variances on level 2 (between subjects). Furthermore, we added the measures of compound nerve action potentials of the median nerve (*CNAP*; Fig. 3a & 3b) and compound muscle action potentials of the M. abductor pollicis brevis (*CMAP*; Fig. 3c & 3d) to the model, in order to control for peripheral variability. On the one hand, both these peripheral measures should relate to stimulus intensity. On the other, there should be no effect of CNAP and CMAP on N20 amplitudes, when statistically controlling for stimulus intensity if the hypothesized fluctuations of excitability emerge on a cortical level. Yet, stimulus-induced thumb twitches may influence the participants´ intensity ratings of the stimuli (even though the stimulated hand was covered with a paper box). The resulting two-level structural equation model (SEM; Fig. 4), indicated statistical significance of all hypothesized effect paths, all $p_\beta \leq .003$, with model fit indices of AIC = 278788.5, BIC = 278972.2, and log-likelihood = -139372.2.

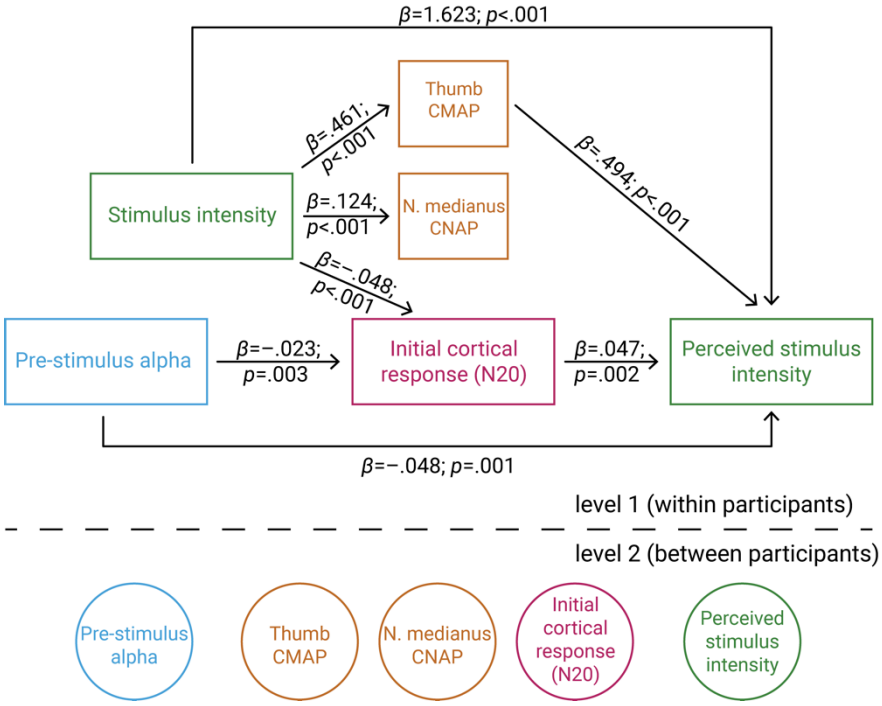

Fig. 4. Multi-level structural equation model of the interplay between pre-stimulus alpha activity, the initial cortical response (N20 component of the SEP), intensity of the presented stimuli, the peripheral control measures CMAP of the M. abductor pollicis brevis and CNAP of the median nerve, as well as the perceived intensity as reported by the participants. Effect paths were estimated between the manifest variables on level 1 (within participants). Latent variables on level 2 served to estimate the respective random intercepts as well as their between-subject variances according to the latent variable approach for multi-level models as implemented in *Mplus*.

To evaluate the model fit, we compared a list of alternative models in- or excluding relevant effect paths (Table 1). As indicated by Chi-Square Difference Tests, the log-likelihood of SEM 1 did not differ from those of SEMs 2-4. Seeking model parsimony, SEM 1 is preferred over SEMs 2-4 since the latter models included one more parameter each, while fitting the data equally well. In comparison to SEMs 5-8, SEM 1 showed a significantly higher log-likelihood suggesting a better model fit than these more parsimonious models. This is further supported by the AIC and BIC values which were altogether lowest for SEM 1. Hence, we conclude that SEM 1 fitted our empirical data best.

The estimated path coefficients (Fig. 4) correspond well with above reported bivariate relationships: When controlling for stimulus intensity, both higher pre-stimulus alpha amplitudes and more negative N20 amplitudes were associated with a lower perceived

intensity (equivalent to a response bias as reflected in *criterion c*), as well as higher pre-stimulus alpha amplitudes co-occurred with more negative N20 amplitudes. In addition, the SEM further dissociated the effects of stimulus intensity on early electrophysiological measures and their respective effects on perceived stimulus intensity. Higher stimulus intensity was associated with larger N20 amplitudes, which constitutes an effect of opposite direction as compared to the N20-related excitability effect on perceived intensity. Furthermore, higher stimulus intensity also led to larger amplitudes of CMAP and CNAP, due to the physical difference in stimulation strength, as could be expected a priori. Additionally, larger CMAP amplitudes resulted in a higher perceived intensity, while no such effect was observed for CNAP. Importantly, neither CMAP nor CNAP related to N20 amplitudes when controlling for stimulus intensity. Thus, fluctuations in cortical processing were not driven by peripheral variability. Finally, a substantial effect on the perceived intensity was found for stimulus intensity. This was expected as the overall accuracy in the discrimination task was about 70%.

Taken together, the SEM confirms the hypothesized influences of instantaneous fluctuations of early somatosensory evoked potentials as well as pre-stimulus oscillatory activity on the consciously accessible percept of a stimulus. Moreover, this analysis demonstrates that stimulus intensity and cortical excitability, which in turn determines the perceived stimulus intensity, show opposing effects on the amplitude of the early SEP.

	Model fit indices					
	AIC diff.	BIC diff.	LL diff.	χ^2 diff.	df diff.	*p* value
(1) Original SEM						
(2) SEM incl. N20 ~ CNAP	1.813	10.166	0.093	0.146	-1	.702
(3) SEM incl. N20 ~ CMAP	0.088	8.441	0.956	0.799	-1	.371
(4) SEM incl. perceived_int ~ CNAP	1.967	10.320	0.016	0.019	-1	.890
(5) SEM excl. perceived_int ~ prestim	8.002	-0.351	-5.001	11.415	1	**< .001**
(6) SEM excl. N20 ~ prestim	15.053	6.701	-8.527	8.087	1	**.005**
(7) SEM excl. N20	47.099	22.040	-26.550	31.095	3	**< .001**
(8) SEM excl. CMAP	9586.906	9570.200	-4795.453	87.030	2	**< .001**

Table 1. Model comparison of SEMs. The original SEM (1) was compared to the alternative models (2-8) using AIC, BIC, log-likelihood (LL), and the Chi-Square Difference Test based on the log-likelihood (with corresponding *p* value). Differences in AIC, BIC, LL, and degrees of freedom (df) were derived by the subtraction *alternative SEM minus SEM 1*. A better model fit is indicated by lower AIC and/or BIC as well as higher LL. The χ^2 difference tests correspond to the comparisons *model with fewer parameters minus model with more parameters*.

Variability in thalamus-related activity is not related to behavioral responses

To scrutinize further whether the observed neuronal effects on the perceived stimulus intensity were of a cortical origin, we further examined the EEG responses prior to the N20 potential. In a sub-sample of 13 participants, the CCA decomposition provided a component that showed a clear peak at 15 ms, characterized by a spatial pattern that suggested a deep, medial source (Fig. 5a & b). Most likely, this CCA component thus corresponds to the P15 potential of the SEP, which is thought to reflect activity in the thalamus (Albe-Fessard et al., 1986). The amplitude of this P15 component did not relate to the perceived stimulus intensity, as examined with a random-intercept linear-mixed-effects model with *perceived intensity* as dependent variable and *P15 amplitude* and *stimulus intensity* as predictors, $\beta_{P15} = .008$,

$z = 0.394$, $p = .694$ ($CI_{95\%}$ of β_{P15}: [-.031, .047]). As expected, *stimulus intensity* however showed a significant effect on *perceived intensity*, $\beta_{stim\_int} = 1.851$, $z = 46.463$, $p < .001$ ($CI_{95\%}$ of β_{stim_int}: [1.773, 1.929]). Additionally, we calculated the statistical power of finding an effect of P15 amplitude in the linear-mixed-effects model, using Monte Carlo simulations (Green & MacLeod, 2016) and assuming an effect size comparable to the observed N20 effect on perceived intensity. The post-hoc power analysis revealed a statistical power of 71.9%. Therefore, we conclude that it is unlikely that the effect of N20 amplitudes on perceived stimulus intensity was driven by thalamic variability and that the modulation of perceived stimulus intensity emerges rather on the cortical level, reflecting instantaneous changes of cortical excitability.

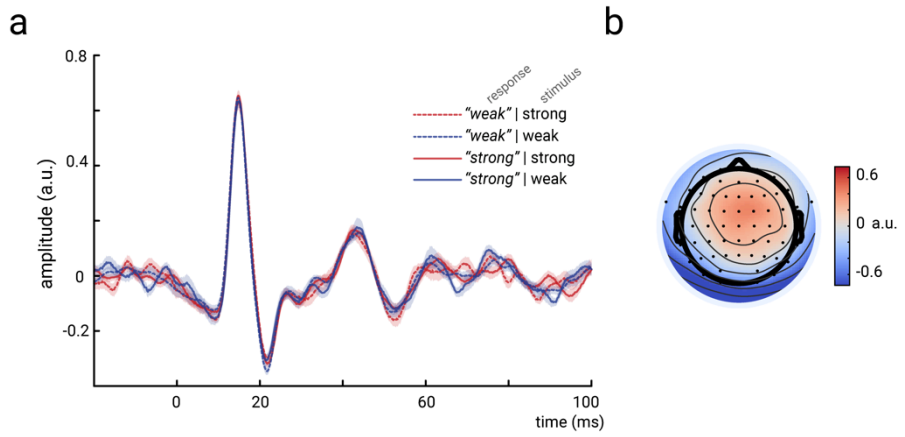

Fig. 5. Thalamic-activity derived from the CCA decomposition. a) Grand-average (N=13) of the thalamic CCA component, showing a clear P15 potential which did not differ across behavioral response categories. Shaded areas correspond to the standard errors of the mean based on the within-subject variances (Morey, 2008). b) Activation pattern of the thalamic CCA component (average across subjects).

3 Discussion

Using a somatosensory discrimination paradigm, we examined the modulation of perceived stimulus intensity by instantaneous fluctuations of cortical excitability at initial cortical processing. Both pre-stimulus alpha band activity and initial cortical evoked responses were associated with a bias in intensity discrimination, suggesting that a lower cortical excitability reduces the perceived intensity of sensory stimuli. Furthermore, we rule out that variability in peripheral nerve activity accounted for these effects, in line with the notion of instantaneous excitability changes being intrinsic to cortical brain dynamics. Intriguingly, elevated excitability and higher presented stimulus intensity resulted in opposing amplitude effects on the initial stimulus-related response in the cortex, the N20 component of the SEP. Based on the neurophysiological principles of the EEG generation, this finding may be explained by a mechanistic link between pre-stimulus alpha activity and initial cortical EPSPs through modulations of resting membrane potentials.

Fluctuations of cortical excitability affect the perceived stimulus intensity

In line with previous studies on the modulatory role of alpha oscillations on perceptual processes (Craddock et al., 2017; Iemi et al., 2017), we found higher pre-stimulus alpha amplitudes to be associated with a lower perceived intensity of somatosensory stimuli. This was indicated both by an increased threshold (*criterion c*) of reporting a higher stimulus intensity according to Signal Detection Theory (Green & Swets, 1966), and by the negative relationship between pre-stimulus alpha amplitude and reported stimulus intensity in the structural equation model. Moreover, sensory processing appeared to be modulated by ongoing oscillatory activity already during initial cortical responses, as suggested by the relations between pre-stimulus alpha activity and N20 amplitude, as well as N20 amplitude and perceived stimulus intensity. The N20 component of the SEP reflects initial stimulus-related excitatory activity (i.e., excitatory post-synaptic potentials; EPSPs) resulting from the

first thalamo-cortical volley to the primary somatosensory cortex (Nicholson Peterson et al., 1995; Wikström et al., 1996; Bruyns-Haylett et al., 2017) and thus represents a direct measure of cortical excitability (when keeping the stimulus intensity constant). The modulation of perceived stimulus intensity therefore relates to a sensory bias at earliest possible cortical processing, reflecting fluctuations of instantaneous neural excitability.

Furthermore, these findings demonstrate that effects of pre-stimulus oscillatory activity on the processing of sensory stimuli are not restricted to near-threshold stimuli where a detection threshold is assumed to be shifted by ongoing brain activity (Iemi et al., 2017; Samaha et al., 2020). Instead, our findings suggest that cortical excitability can affect the representation of stimulus features in supra-threshold perception, too. Importantly, our criterion-free discrimination paradigm of two neutral response alternatives ("strong" or "weak") precluded the potential confounding effect of perceptual confidence, which has recently been considered as an alternative explanation for pre-stimulus alpha effects on perceptual biases (Samaha et al., 2017; Benwell et al., 2017). In our forced-choice paradigm, different levels of perceptual confidence could not have influenced the intensity ratings since the task was to distinguish two clearly perceptible stimuli, and not to report whether a stimulus was perceived or not (as done in near-threshold paradigms). Thus, the current findings unequivocally indicate– to the best of our knowledge for the first time – that pre-stimulus alpha oscillations affect the behavioral outcome via a modulation of the internally represented stimulus intensity.

Opposing signatures of presented stimulus intensity and excitability in the early SEP

Following the hypothesis of higher alpha activity being associated with lower cortical excitability (Klimesch et al., 2007; Jensen & Mazaheri, 2010; Samaha et al., 2020), it may seem counter-intuitive that higher alpha amplitudes were associated with larger (i.e., more negative) N20 amplitudes in our data. However, as we proposed recently (Stephani et al.,

2020), this relationship may be explained by the neurophysiological mechanisms of EEG generation. The generated voltage on the scalp, U, in our case relating to the N20 potential, can be defined in the following way (Kandel et al., 2000; Lopes da Silva, 2004; Ilmoniemi & Sarvas, 2019):

$$U \sim I * N_{neurons} * LF$$

where I denotes the sum of local primary post-synaptic currents due to the activation of a given neuron, $N_{neurons}$ the number of involved neurons, and LF the lead field coefficient projecting source activity to the electrodes on the scalp. Since the spatial arrangement of the neural generators and the EEG sensors was stable across stimulation events, LF reflects a constant in the measurement of the N20 potential. In contrast, $N_{neurons}$ should increase with stimulus intensity since more nerve fibers are excited at stimulation site when applying stimuli of higher currents. This should lead to an increase of SEP amplitude with stimulus intensity, as reported in previous studies (Klostermann et al., 1998; Jousmäki & Forss, 1998) and as was observed in the current dataset for cortical (Fig. 2d) as well as peripheral responses (Fig. 3b & 3d). For constant stimulus intensity, however, $N_{neurons}$ is expected to stay approximately constant and amplitudes in the EEG should primarily depend on I, reflecting excitatory post-synaptic currents (EPSCs) in case of the N20 component. Crucially, EPSCs directly depend on the electro-chemical driving forces produced by the membrane potential. When moving the membrane potential towards depolarization – a state of higher excitability – the electro-chemical driving force for further depolarizing inward trans-membrane currents is decreased (Castro-Alamancos, 2009), which leads to smaller EPSCs (Deisz et al., 1991), and should in turn result in smaller amplitudes of the scalp EEG. Assuming an inverse relationship between the amplitude of alpha oscillations and neuronal excitability (as for example indicated by a lower neural firing rate during higher alpha activity; Haegens et al., 2011), one should hence rather expect *decreased* N20 amplitudes following *low* pre-stimulus alpha activity. This is what was observed in our data when controlling for stimulus intensity (Fig. 4).

Moreover, the notion of smaller (i.e., less negative) N20 amplitudes reflecting a state of higher excitability is corroborated by the behavioral data: When controlling for stimulus intensity, we found less negative N20 amplitudes to be associated with higher perceived stimulus intensity.

Taken together, our findings thus demonstrate that the intensity of the presented stimulus and the degree of instantaneous neural excitability are jointly reflected in the early SEP but with opposing signatures: While stronger stimulus intensity increases the N20 potential, *decreased* N20 amplitudes appear to be associated with an *increase* in excitability (which in turn lead to a higher perceived stimulus intensity). This challenges the prevailing, prominent assumption that the amplitude of brain potentials, especially at early processing stages, reflects the coding of the perceived stimulus intensity. Rather, our findings call for a more differentiated view. Although the amplitude of early event-related potentials may indeed reflect the size of the input (e.g., a stronger or weaker somatosensory stimulus), the neural evaluation of this input (i.e., the perceived intensity), however, further depends on internal neural states, such as neural excitability, which may even reverse the amplitude effects of the input already at the earliest cortical processing stages.

Origin of excitability fluctuations

To further narrow down the neuronal sources that eventually led to fluctuations of the perceptual outcome, we controlled for peripheral nerve variability, extracted spatially well-defined EEG potentials, and examined subcortical activity.

Variability in afferent peripheral activity, as measured by compound nerve action potentials (CNAP) at the upper arm, did not influence the perceived stimulus intensity when controlling for stimulus intensity. However, a robust effect on the perceived stimulus intensity was observed for efferent peripheral activity, as measured by compound muscle action potentials (CMAP) of the M. abductor pollicis brevis. This may be explained by differences in

proprioceptive sensations associated with the thumb twitches elicited by the stimulation, whose extent may depend on changes of the prevailing muscle tonus. Importantly, neither the CNAP nor the CMAP measure related to cortical excitability as measured by the N20 component. Thus, the excitability effects in the early SEP are distinct from variability in peripheral nerve activity.

Furthermore, pre-stimulus alpha band activity and the N20 component of the SEP were retrieved from the same neuronal sources, which – as indicated by source reconstruction – were localized in the primary sensory cortex, centered around the hand region of Brodmann area 3b. Although one should bear in mind the limited spatial resolution of EEG, this further supports the notion of excitability fluctuations in primary sensory regions of the cortex, being reflected both in ongoing and evoked neural activity.

Another possibility is that already subcortical sources – particularly in the thalamus – may play a role in modulating sensory excitability and hence shape the perceptual outcome (Kosciessa et al., 2020). Yet, our analyses of the thalamus-related P15 component did not support this notion. Given the acceptable statistical power of these analyses, we conclude that the modulation of perceived intensity in somatosensory stimulation has its neuronal origin at the cortical level.

However, it remains an open question whether the observed excitability changes reflect local or global neural dynamics. Although there is initial evidence that cortical excitability may be organized temporally in a scale-free manner (Stephani et al., 2020), which may reflect an embedding into global critical-state dynamics (Beggs & Plenz, 2003; Palva et al., 2013; Avramiea et al., 2020), future work has to examine the spatial organization of excitability more specifically across different somatotopic projections in primary sensory areas as well as across diverse brain regions.

Conclusions

Both ongoing oscillatory alpha activity as well as amplitude fluctuations of the first cortical response shape the perceived intensity of somatosensory stimuli. These effects most likely reflect instantaneous changes of cortical excitability in the primary somatosensory regions of the cortex, leading to a sensory bias which manifests already during the very first cortical response. Challenging the common view of how the evaluation of stimulus intensity is reflected in brain potentials, cortical excitability and the presented stimulus intensity were associated with opposing effects on the early SEP. We argue that this disparity may be explained by a mechanistic link between ongoing oscillations and stimulus evoked activity through membrane potential alterations. This sheds new light on the neural correlates of the intensity encoding of somatosensory stimuli, which may well apply to other sensory domains, too.

4 Methods

Participants

A total of 32 subjects (all male, mean age = 27.0 years, *SD* = 5.0) were recruited from the database of the Max Planck Institute for Human Cognitive and Brain Sciences, Leipzig, Germany. As assessed using the Edinburgh Handedness Inventory (Oldfield, 1971), all participants were right-handed (lateralization score, *M* = +93.1, *SD* = 11.6). No participant reported any neurological or psychiatric disease. All participants gave informed consent and were reimbursed monetarily. The study was approved by the local ethics committee (Ethical Committee at the Medical Faculty of Leipzig University, 04006 Leipzig, Germany).

Stimuli

Somatosensory stimuli were applied using electrical stimulation of the median nerve. A non-invasive bipolar stimulation electrode was positioned on the left wrist (cathode proximal). The electrical stimuli were designed as squared pulses of a 20-µs duration and applied using a DS-7 constant-current stimulator (Digitimer, Hertfordshire, United Kingdom). Stimuli of two intensities were presented, in the following referred to as *weak* and *strong* stimulus. The intensity of the weak stimulus was set to 1.2 times the motor threshold, leading to a clearly visible thumb twitch for every stimulus. The individual motor threshold was determined as the lowest intensity for which a thumb twitch was visible to the experimenter, as determined by a staircase procedure. The intensity of the strong stimulus was adjusted during training blocks prior to the experiment so that it was barely above the *just-noticeable difference*, corresponding to a discrimination sensitivity of about *d'* = 1.5 according to Signal Detection Theory (SDT; Green & Swets, 1966). Thus, the stimulation intensities of the two stimuli were only barely distinguishable (despite both being clearly perceivable), with average intensities of 6.60 mA (*SD* = 1.62) and 7.93 mA (*SD* = 2.06), for the weak and strong stimulus, respectively.

Procedure

During the experiment, participants were seated comfortably in a chair their hands extended in front of them in the supinate position on a pillow. The left hand and wrist, to which the stimulation electrodes were attached, was covered with a paper box in order to prevent the participants to judge the stimulus intensity visually by the extent of thumb twitches elicited by the stimulation. Weak and strong stimuli were presented with an equal probability in a continuous, pseudo-randomized sequence with inter-stimulus intervals (ISI) ranging from 1463 to 1563 ms (randomly drawn from a uniform distribution; $ISI_{average}$ = 1513 ms). In total, 1000 stimuli were applied, divided into five blocks of 200 stimuli each with short breaks in between. Participants were to indicate after each stimulus whether it was the weak or strong stimulus, by button press with their right index and middle fingers as fast as possible. The button assignment for weak and strong stimulus was balanced across participants. Furthermore, every sequence started with a weak stimulus in order to provide an anchor point for the intensity judgments (participants were informed about this). While performing the discrimination task, participants were instructed to fixate their gaze on a cross on a computer screen in front of them.

Prior to the experiment, training blocks of 15 stimuli each were run in order to familiarize the participants with the task and to individually adjust the intensity of the strong stimulus so that a discrimination sensitivity of about d'=1.5 resulted (the intensity of the weak stimulus was set at 1.2 times the motor threshold for all participants). On average across participants, this procedure comprised 10.5 training blocks (SD=5.8). During these training blocks, participants were provided with visual feedback of their response accuracy. No information on task performance was given during the experimental blocks.

Data Acquisition

EEG data were recorded from 60 Ag/AgCl electrodes at a sampling rate of 5000 Hz using an 80-channel EEG system (NeurOne, Bittium, Oulu, Finland). A built-in band-pass filter in the frequency range from 0.16 to 1250 Hz was used. Electrodes were mounted in an elastic cap (EasyCap, Herrsching, Germany) at the international 10-10 system positions FP1, FPz, FP2, AF7, AF3, AFz, AF4, AF8, F7, F5, F3, F1, Fz, F2, F4, F6, F8, FT9, FT7, FT8, FT10, FC5, FC3, FC1, FC2, FC4, FC6, C5, C3, C1, Cz, C2, C4, C6, CP5, CP3, CP1, CPz, CP2, CP4, CP6, T7, T8, TP7, TP8, P7, P5, P3, P1, Pz, P2, P4, P6, P8, PO7, PO3, PO4, PO8, O1, and O2, with FCz as the reference and POz as the ground. For the purpose of source reconstruction, the electrode positions were measured in 3D space individually for each subject using the Polhemus Patriot motion tracker (Polhemus, Colchester, Vermont). In order to record the electrooculogram (EOG), four additional electrodes were positioned at the outer canthus and the infraorbital ridge of each eye. The impedances of all electrodes were kept below 10 kΩ. For source reconstruction, EEG electrode positions were measured in 3D space individually for each subject using Polhemus Patriot (Polhemus, Colchester, Vermont). Additionally, the compound nerve action potential (CNAP) of the median nerve and the compound muscle action potential (CMAP) of the M. abductor pollicis brevis were measured. For the CNAP, two bipolar electrodes were positioned on the inner side of the left upper arm along the path of the median nerve, at a distance of about 1 cm (reference electrode distal). The CMAP was measured from two bipolar electrodes placed on the stimulated hand, one on the muscle belly of the M. abductor pollicis brevis and the other on the second joint of the thumb (reference electrode).

Structural T1-weighted MRI scans (MPRAGE) of all participants but two were obtained from the database of the Max Planck Institute for Human Cognitive and Brain Sciences, Leipzig, Germany, acquired within the same year of the experiment or up to 3 years

earlier on a 3T Siemens Verio, Siemens Skyra or Siemens Prisma scanner (Siemens, Erlangen, Germany).

EEG pre-processing

Stimulation artifacts were cut out and interpolated between -2 to 4 ms relative to stimulus onset using Piecewise Cubic Hermite Interpolating Polynomials (MATLAB function *pchip*). The EEG data were band-pass filtered between 30 and 200 Hz, sliding a 4th order Butterworth filter forwards and backwards over the data to prevent phase shift (MATLAB function *filtfilt*). As outlined in a previous study (Stephani et al., 2020), this filter allowed to specifically focus on the N20-P35 complex of the SEP, which emerges from frequencies above 35 Hz, and to omit contributions of later (slower) SEP potentials of no interest. Additionally, this filter effectively served as baseline correction of the SEP since it removed slow trends in the data, reaching an attenuation of 30 dB at 14 Hz, thus ensuring that fluctuations in the SEP did not arise from fluctuations within slower frequencies (e.g., alpha band activity). Subsequently, segments of the data that were distorted by muscle or non-biological artifacts were removed by visual inspection. After re-referencing to an average reference, eye artefacts were removed using independent component analysis (Infomax ICA) whose weights were calculated on the data band-pass filtered between 1 and 45 Hz (4th order Butterworth filter applied forwards and backwards). For SEP analysis, the data were segmented into epochs from -100 to 600 ms relative to stimulus onset, resulting in about 995 trials on average per participant. EEG pre-processing was performed using EEGLAB (Delorme & Makeig, 2004), and custom written scripts in MATLAB (The MathWorks Inc., Natick, Massachusetts).

Single-trial extraction using CCA

Single-trial SEPs were extracted using Canonical Correlation Analysis (CCA), as proposed by Waterstraat et al. (2015), and in the same way applied as described in Stephani et al. (2020) for a similar dataset.

CCA finds the spatial filters $\boldsymbol{w}_x$ and $\boldsymbol{w}_y$ for multi-channel signals $\boldsymbol{X}$ and $\boldsymbol{Y}$ by solving the following optimization problem for maximizing the correlation:

$$\max_{w_x, w_y} corr(\boldsymbol{w}_x^T \boldsymbol{X}, \boldsymbol{w}_y^T \boldsymbol{Y})$$

where $\boldsymbol{X}$ is a multi-channel signal constructed from concatenating all the epochs of a subject's recording, i.e. $\boldsymbol{X} = [\boldsymbol{x}_1, \boldsymbol{x}_2, \dots, \boldsymbol{x}_N]$ with $\boldsymbol{x}_i \in \mathbb{R}^{channel \times time}$ being the multi-channel signal of a single trial and N the total number of trials. Additionally, $\boldsymbol{Y} = \underbrace{[\overline{\boldsymbol{x}}, \dots, \overline{\boldsymbol{x}}]}_{\boldsymbol{N\ times}}$ with $\overline{\boldsymbol{x}} = \frac{1}{N}\sum_{i=1}^{N} \boldsymbol{x}_i$ denoting the grand average of all trials. Since averaging cancels the background noise and recovers the shared morphology of the SEP of interest among all the trials, the CCA procedure resembles a template matching between the single trial signals and the template time signature of the SEP of interest. The spatial filter $\boldsymbol{w}_x$ provides us with a vector of weights for mixing the channels of each single trial (i.e. $\boldsymbol{x}_{i,CCA} = \boldsymbol{w}_x^T \boldsymbol{x}_i$) and recovering their underlying SEP. Therefore, $\boldsymbol{w}_x$ can be interpreted as the spatial signature of the SEP of interest across all single trials. The optimization problem of CCA can be solved using eigenvalue decomposition. Therefore, multiple CCA spatial components can be extracted for each subject, being the eigenvectors of the corresponding eigenvalue decomposition. Since we are mainly interested in the early portion of the SEP, the two signal matrices $\boldsymbol{X}$ and $\boldsymbol{Y}$ were constructed using shorter segments from 5 to 80 ms post-stimulus. The extracted CCA spatial filter was, however, applied to the whole-length epochs from -100 to 600 ms. The signal resulting from mixing the single trial's channels using the CCA spatial filter $\boldsymbol{w}_x$, i.e. $\boldsymbol{x}_{i,CCA} = \boldsymbol{w}_x^T \boldsymbol{x}_i$, is called a CCA component of that trial.

The spatial activity pattern of each CCA component was computed by multiplying the spatial filters $\boldsymbol{w}_x$ by the covariance matrix of $\boldsymbol{X}$, as $cov(\boldsymbol{X})\boldsymbol{w}_x$, in order to take the noise structure of the data into account (Haufe et al., 2014). The CCA components whose spatial patterns showed a pattern of a tangential dipole over the central sulcus (typical for the N20-P35 complex) were selected for further analyses and referred to as *tangential CCA components*. Such a tangential CCA component was present in all subjects among the first two CCA components with the maximum canonical correlation coefficients. Since CCA solutions are insensitive to the polarity of the signal, we standardized the resulting tangential CCA components by multiplying the spatial filter by a sign factor, in the way that the N20 potential always appeared as a negative peak in the SEP.

Furthermore, in a sub-sample of 13 subjects, a CCA component could be identified among the first four CCA components, that showed a peak at around 15 ms post-stimulus (presumably the P15 component of the SEP) and a spatial pattern that was characterized by a central, outspread activation (in the following referred to as *thalamic CCA component*). Also here, the CCA components were standardized so that the P15 always appeared as a positive peak.

SEP peak amplitudes and pre-stimulus oscillatory activity

N20 peak amplitudes were defined as the minimum value in single-trial SEPs of the tangential CCA components ±2 ms around the latency of the N20 in the within-subject average SEP. P15 amplitudes were measured from the thalamic CCA components as the average amplitude in a time window ±1 ms around the latency of the P15 in the within-subject average SEP.

To estimate the average amplitude of pre-stimulus alpha band activity, the data were segmented from -500 to -5 ms relative to stimulus onset and band-pass filtered between 8 and 13 Hz, using a 4th order Butterworth filter (applied forwards and backwards). In order to avoid

filter-related edge artifacts, the data segments were mirrored before filtering to both sides (symmetric padding). Segmenting the data before filtering prevented any leakage from post-stimulus signals to the pre-stimulus time window. In order to examine pre-stimulus alpha band activity of the same sources as of the SEP, the spatial filter of the tangential CCA component was also applied to the pre-stimulus alpha data. Subsequently, the amplitude envelope of the extracted alpha oscillations was computed by taking the absolute value of the analytic signal, using Hilbert transform of the real-valued signal. To derive one pre-stimulus alpha metric for every trial, amplitudes of the alpha envelope were averaged in the pre-stimulus time window of interest between -200 and -10 ms and log-transformed for subsequent statistical analyses in order to approximate a normal distribution.

EEG source reconstruction

Sources of the EEG signal were reconstructed using lead field matrices based on individual brain anatomies and individually measured electrode positions. Structural T1-weighted MRI images (MPRAGE) were segmented using the Freesurfer software (http://surfer.nmr.mgh.harvard.edu/), and a three-shell boundary element model (BEM) based on the segmented MRI was used to compute the lead field matrix with OpenMEEG (Kybic et al., 2005; Gramfort et al., 2010). A template brain anatomy (ICBM152; Fonov et al., 2009) was used for two subjects for whom no individual MRI scans were available. Additionally, standard electrode positions were used for one subject for whom the 3D digitization of the electrode positions was corrupted. The lead field matrices were inverted using the eLORETA method (Pascual-Marqui, 2007), and sources were reconstructed for the spatial patterns of the tangential CCA component of every subject. For group-level analysis, we projected the individual source estimates onto the ICBM152 template anatomy using the spherical co-registration with the FSAverage template (Fischl et al., 1999) derived from Freesurfer. Subsequently, the source estimates were averaged across subjects. Brainstorm (Tadel et al.,

2011) was used for building individual head models and visualizing the source space data. The MATLAB implementation of the eLORETA algorithm was derived from the MEG/EEG Toolbox of Hamburg (METH; https://www.uke.de/english/departments-institutes/institutes/neurophysiology-and-pathophysiology/research/research-groups/index.html).

Processing of peripheral electrophysiological data (median nerve CNAP and thumb CMAP)

Analogously to the EEG data, stimulation artifacts were cut out and interpolated between -2 to 4 ms relative to stimulus-onset using Piecewise Cubic Hermite Interpolating Polynomials. To achieve a sufficient signal-to-noise ratio (SNR) of the short-latency CNAP peak of only a few milliseconds duration on single-trial level, the data were high-pass filtered at 70 Hz (4^{th} order Butterworth filter applied forwards and backwards). For the CMAP, no further filtering was necessary given the naturally high SNR of muscle potentials (mV range). Here, only a baseline correction was performed from -20 to -5 ms to account for slow potential shifts. For the CNAP, single-trial peak amplitudes were extracted as the maximum amplitude ±1 ms around the participant-specific latency of the CNAP peak that was found between 5 and 9 ms in the within-participant averages. The CMAP was evaluated regarding its peak-to-peak amplitude, which was defined as the difference between the minimum and maximum amplitude measured ±1 ms around the participant-specific latencies of the negative and positive peaks of the biphasic CMAP response (which were found between 5 and 11 ms as well as 10 to 20 ms in the within-participant averages, respectively).

Signal Detection Theory (SDT)

In order to separate the discrimination ability of the two stimulus intensities from a general response bias, we applied Signal Detection Theory (SDT; Green & Swets, 1966; Kingdom & Prins, 2016). The ability to discriminate the two stimulus intensities was quantified using *sensitivity d'*, as calculated in the following way:

$$d' = \phi^{-1}(p("strong" \mid strong)) - \phi^{-1}(p("strong" \mid weak))$$

where ϕ^{-1} corresponds to the inverse of the cumulative normal distribution, $p("strong" \mid strong)$ to the probability of strong stimuli being rated as strong stimuli, and $p("strong" \mid weak)$ to the probability of weak stimuli being rated as strong stimuli. Response probabilities were calculated as the number of responses divided by the number of stimuli of the respective categories. The response bias, *criterion c*, was calculated as follows:

$$c = -0.5 * (\phi^{-1}(p("strong" \mid strong)) + \phi^{-1}(p("strong" \mid weak))) .$$

According to Signal Detection Theory, *sensitivity d'* here represents the distance between the distributions of the internal responses of the two stimuli, and thus reflects the discriminability between strong and weak stimulus intensity. *Criterion c* reflects the internal threshold above which a stimulus is rated as strong stimulus and below which a stimulus is rated as weak stimulus, thus representing a general response bias. With respect to our data, a higher *criterion c* therefore indicates a general tendency to report lower stimulus intensities.

Statistical analyses

To confirm that task accuracy was above chance level, we ran non-parametric permutation tests (Crowley, 1992). Within each participant, we derived a null distribution of chance-level performance by randomly remapping the behavioral responses with the presented stimuli 100,000 times (Combrisson & Jerbi, 2015). The *p* value of the empirical task accuracy was calculated as the proportion of higher accuracy values in the surrogate data. Bonferroni correction was applied to account for the multiple tests across participants.

The effects of the SEP measures *pre-stimulus alpha amplitude* and *N20 peak amplitude* on the SDT measures *sensitivity d'* and *criterion c* were examined using a binning approach: First, trials were sorted according to the amplitudes of the EEG measures. Next, the SDT measures corresponding to the first and fifth quintile of the sorted trials were compared using paired-sample *t*-tests. To quantify effect sizes, *Cohen's d* was calculated as the mean

difference between the dependent samples divided by the standard deviation of differences between the dependent samples.

The relationship between pre-stimulus alpha activity and the N20 component was tested using a random-slope linear mixed effects model with *pre-stimulus alpha amplitude* as predictor of *N20 peak amplitude*, and *subject* as random factor:

$$N20\ peak\ amplitude \sim 1 + pre\text{-}stimulus\ alpha + (1 + pre\text{-}stimulus\ alpha \mid subject)\ .$$

The relationship between thalamus-related activity and intensity perception was tested using a random-intercept linear-mixed-effects model with *P15 amplitude* and *presented stimulus intensity* as predictors of *perceived stimulus intensity*, as well as *subject* as random factor:

$$Perceived\ stimulus\ intensity \sim 1 + P15\ amplitude + presented\ stimulus\ intensity + (1 + \mid subject)\ .$$

Here, a logit link function was used to account for the dichotomous scale of *perceived stimulus intensity*. Furthermore, we conducted a post-hoc power analysis to evaluate the probability of finding an effect of P15 amplitude on perceived stimulus intensity if it was existent. For this, we used Monte Carlo simulations with 1000 permutations based on the empirical dataset (Green & MacLeod, 2016), assuming an effect size of $\beta = .05$, which is in the range of the observed effect of N20 amplitude on perceived stimulus intensity.

In addition, the interrelation of pre-stimulus alpha activity, the N20 component of the SEP, peripheral nerve activity as measured by CNAP and CMAP, the presented stimulus intensity, as well as the perceived stimulus intensity were examined using confirmatory path analysis based on multi-level structural equation modeling as implemented in the general latent variable framework of *Mplus* (Muthén & Muthén, 1998-2017). *Pre-stimulus alpha amplitude* and *presented stimulus intensity* were included as exogenous variables, *N20 peak amplitude*, *CNAP amplitude*, *CMAP amplitude*, and *perceived stimulus intensity* as

endogenous variables. The relationships contained in the hypothesized model are summarized in Table 2. Trials with no behavioral response were excluded from the analysis. In total, 31,347 single trials were included in the SEM, with 979.6 trials on average per participant. Model parameters were estimated using the MLR estimator provided by *Mplus*, a maximum-likelihood estimator robust to violations of the assumption of normally distributed data. A logit link function was used to account for the dichotomous scale of *perceived stimulus intensity*. The fit of the hypothesized model was examined comparing it to alternative models constructed by stepwise in- or excluding relevant effect paths (Table 1). Model comparisons were evaluated using χ^2 difference tests based on the log-likelihood (Muthén, 1998-2004), the Akaike Information Criterion (AIC), and the Bayesian Information Criterion (BIC). (Note that no other fit indices, such as CFI, RMSEA or SRMR are available for our type of model with a multi-level structure and a dichotomous outcome variable.)

Level 1 (within participants):
N20 amplitude ~ 1 + stimulus intensity + pre-stimulus alpha
CNAP ~ 1 + stimulus intensity
CMAP ~ 1 + stimulus intensity
Perceived intensity ~ 1 + stimulus intensity + N20 amplitude + pre-stimulus alpha + CMAP
Level 2 (between participants):
N20 amplitude ~~ N20 amplitude
CNAP ~~ CNAP
CMAP ~~ CMAP
Perceived intensity ~~ perceived intensity
Pre-stimulus alpha ~~ pre-stimulus alpha

Table 2. Relationships included in the hypothesized SEM. Level 1 equations reflect the within-participant effects between variables of interest. On level 2, only intercepts and variances of each variable were modelled; apart from *stimulus intensity* which only varied within participants by experimental design.

For all analyses, the statistical significance level was set to $p = .05$ (two-sided). Correspondingly, two-sided confidence intervals were calculated with a confidence level of .95 ($CI_{95\%}$). The permutation-based analyses and *t*-tests were performed in MATLAB (version 2019b, The MathWorks Inc., Natick, Massachusetts). For both the linear-mixed-effects model and the structural equation models, all continuous variables (i.e., pre-stimulus alpha, N20 amplitude, CNAP, and CMAP) were z-transformed prior to statistics. The linear-mixed-effects model was calculated in R (version 3.5.3, R Core Team, 2018) with the *lmer* function of the *lme4* package (version 1.1-23, Bates et al., 2015), estimating the fixed-effect coefficients based on Maximum Likelihood (ML). To derive a *p* value for the fixed-effect coefficients, the denominator degrees of freedom were adjusted using Satterthwaite´s method (Satterthwaite, 1946) as implemented in the R package *lmerTest* (version 3.1-2, Kuznetsova et al., 2017). Structural equation modelling was performed in *Mplus* (version 8.4 Demo, Base Program and Combination Add-On; Muthén & Muthén, 1998-2017) using the *MplusAutomation* package in R for scripting (Hallquist & Wiley, 2018). Post-hoc power analyses were performed using the R package *simr* (Green & MacLeod, 2016).

Data availability

The data that supports the findings of this study are available upon request from the corresponding author (T.S.; stephani@cbs.mpg.de). The data cannot be made available in a public repository due to the privacy policies for human biometric data according to the European General Data Protection Regulation (GDPR).

Code availability

The custom-written code that was used for data processing and statistical analyses is publicly available at https://osf.io/v9xa6/?view_only=3428139b7ab94824bac0eff0b4b92cc5.

Acknowledgements

V.V.N. was supported in part by the HSE Basic Research Program and the Russian Academic Excellence Project 5-100. We thank Sylvia Stasch for participant recruitment and help with data collection.

Author contributions

T.S., V.V.N., and A.V. designed research; T.S. performed research; T.S. and A.H. analyzed data; T.S. wrote the first draft of the paper; T.S. and V.V.N. wrote the paper; T.S., A.H., M.J.I., A.V., and V.V.N. edited the paper; M.J.I. contributed unpublished reagents/analytic tools.

Competing Interests statement

The authors declare no competing financial interests.

References

Albe-Fessard, D., Tasker, R., Yamashiro, K., Chodakiewitz, J., & Dostrovsky, J. (1986). Comparison in man of short latency averaged evoked potentials recorded in thalamic and scalp hand zones of representation. *Electroencephalography and Clinical Neurophysiology/Evoked Potentials Section*, *65*, 405–415.

Allison, T., McCarthy, G., Wood, C. C., & Jones, S. J. (1991). Potentials Evoked in Human and Monkey Cerebral Cortex by Stimulation of the Median Nerve. *Brain*, *114*, 2465–2503.

Arieli, A., Sterkin, A., Grinvald, A., & Aertsen, A. (1996). Dynamics of ongoing activity: Explanation of the large variability in evoked cortical responses. *Science*, *273*, 1868–1871.

Avramiea, A.-E., Hardstone, R., Lueckmann, J.-M., Bím, J., Mansvelder, H. D., & Linkenkaer-Hansen, K. (2020). Pre-stimulus phase and amplitude regulation of phase-locked responses are maximized in the critical state. *eLife*, *9*, e53016.

Bates, D., Mächler, M., Bolker, B., & Walker, S. (2015). Fitting Linear Mixed-Effects Models Using lme4. *Journal of Statistical Software*, *67*, 1–48.

Baumgarten, T. J., Schnitzler, A., & Lange, J. (2016). Prestimulus Alpha Power Influences Tactile Temporal Perceptual Discrimination and Confidence in Decisions. *Cerebral Cortex*, *26*, 891–903.

Beggs, J. M., & Plenz, D. (2003). Neuronal Avalanches in Neocortical Circuits. *The Journal of Neuroscience*, *23*, 11167–11177.

Benwell, C. S. Y., Tagliabue, C. F., Veniero, D., Cecere, R., Savazzi, S., & Thut, G. (2017). Prestimulus EEG power predicts conscious awareness but not objective visual performance. *eNeuro*, *4*, ENEURO.0182-17.2017.

Bollimunta, A., Mo, J., Schroeder, C. E., & Ding, M. (2011). Neuronal mechanisms and attentional modulation of corticothalamic α oscillations. *The Journal of Neuroscience*, *31*, 4935–4943.

Bruyns-Haylett, M., Luo, J., Kennerley, A. J., Harris, S., Boorman, L., Milne, E., Vautrelle, N., Hayashi, Y., Whalley, B. J., Jones, M., Berwick, J., Riera, J., & Zheng, Y. (2017). The neurogenesis of P1 and N1: A concurrent EEG/LFP study. *NeuroImage*, *146*, 575–588.

Busch, N. A., Dubois, J., & VanRullen, R. (2009). The phase of ongoing EEG oscillations predicts visual perception. *The Journal of Neuroscience*, *29*, 7869–7876.

Castro-Alamancos, M. A. (2009). Cortical up and activated states: implications for sensory information processing. *The Neuroscientist*, *15*, 625–634.

Combrisson, E., & Jerbi, K. (2015). Exceeding chance level by chance: The caveat of theoretical chance levels in brain signal classification and statistical assessment of decoding accuracy. *Journal of neuroscience methods*, *250*, 126–136.

Craddock, M., Poliakoff, E., El-Deredy, W., Klepousniotou, E., & Lloyd, D. M. (2017). Pre-stimulus alpha oscillations over somatosensory cortex predict tactile misperceptions. *Neuropsychologia*, *96*, 9–18.

Crowley, P. (1992). Resampling Methods for Computation-Intensive Data Analysis in Ecology and Evolution. *Annual Review of Ecology and Systematics*, *23*, 405–447.

Deisz, R. A., Fortin, G., & Zieglgansberger, W. (1991). Voltage dependence of excitatory postsynaptic potentials of rat neocortical neurons. *Journal of neurophysiology*, *65*, 371–382.

Delorme, A., & Makeig, S. (2004). EEGLAB: An open source toolbox for analysis of single-trial EEG dynamics including independent component analysis. *Journal of neuroscience methods*, *134*, 9–21.

Fedele, T., Scheer, H.-J., Burghoff, M., Waterstraat, G., Nikulin, V. V., & Curio, G. (2013). Distinction between added-energy and phase-resetting mechanisms in non-invasively detected somatosensory evoked responses. *Conference proceedings: IEEE Engineering in Medicine and Biology Society. Annual Conference*, *2013*, 1688–1691.

Fischl, B., Sereno, M. I., Tootell, R. B.H., & Dale, A. M. (1999). High-resolution intersubject averaging and a coordinate system for the cortical surface. *Human Brain Mapping*, *8*, 272–284.

Fonov, V. S., Evans, A. C., McKinstry, R. C., Almli, C. R., & Collins, D. L. (2009). Unbiased nonlinear average age-appropriate brain templates from birth to adulthood. *NeuroImage*, *47*, S102.

Forschack, N., Nierhaus, T., Müller, M. M., & Villringer, A. (2020). Dissociable neural correlates of stimulation intensity and detection in somatosensation. *NeuroImage*, 116908.

Gramfort, A., Papadopoulo, T., Olivi, E., & Clerc, M. (2010). OpenMEEG: opensource software for quasistatic bioelectromagnetics. *Biomedical engineering online*, *9*, 45.

Green, D. M., & Swets, J. A. (1966). *Signal detection theory and psychophysics*. New York, NY: Wiley.

Green, P., & MacLeod, C. J. (2016). SIMR an R package for power analysis of generalized linear mixed models by simulation. *Methods in Ecology and Evolution*, *7*, 493–498.

Haegens, S., Nácher, V., Luna, R., Romo, R., & Jensen, O. (2011). α-Oscillations in the monkey sensorimotor network influence discrimination performance by rhythmical inhibition of neuronal spiking. *Proceedings of the National Academy of Sciences of the United States of America*, *108*, 19377–19382.

Hallquist, M. N., & Wiley, J. F. (2018). MplusAutomation: An R Package for Facilitating Large-Scale Latent Variable Analyses in Mplus. *Structural Equation Modeling: A Multidisciplinary Journal*, *25*, 621–638.

Haufe, S., Meinecke, F., Görgen, K., Dähne, S., Haynes, J.-D., Blankertz, B., & Bießmann, F. (2014). On the interpretation of weight vectors of linear models in multivariate neuroimaging. *NeuroImage*, *87*, 96–110.

Iemi, L., Chaumon, M., Crouzet, S. M., & Busch, N. A. (2017). Spontaneous Neural Oscillations Bias Perception by Modulating Baseline Excitability. *The Journal of Neuroscience*, *37*, 807–819.

Ilmoniemi, R., & Sarvas, J. (2019). *Brain signals: Physics and mathematics of MEG and EEG*. Cambridge: The MIT Press.

Jensen, O., & Mazaheri, A. (2010). Shaping functional architecture by oscillatory alpha activity: Gating by inhibition. *Frontiers in human neuroscience*, *4*, 186.

Jousmäki, V., & Forss, N. (1998). Effects of stimulus intensity on signals from human somatosensory cortices. *Neuroreport*, *9*, 3427–3431.

Kandel, E. R., Schwartz, J. H., & Jessell, T. M. (Eds.) (2000). *Principles of neural science.* (4. ed.). New York, NY: McGraw-Hill Health Professions Division.

Kingdom, F. A. A., & Prins, N. (2016). *Psychophysics: A practical introduction.* (Second edition). Elsevier science & technology books. London: Elsevier Academic Press.

Klimesch, W., Sauseng, P., & Hanslmayr, S. (2007). EEG alpha oscillations: The inhibition-timing hypothesis. *Brain research reviews*, *53*, 63–88.

Klostermann, F., Nolte, G., Losch, F., & Curio, G. (1998). Differential recruitment of high frequency wavelets (600 Hz) and primary cortical response (N20) in human median nerve somatosensory evoked potentials. *Neuroscience letters*, *256*, 101–104.

Kosciessa, J. Q., Lindenberger, U., & Garrett, D. D. (2020). Thalamocortical excitability adjustments guide human perception under uncertainty. *bioRxiv*.

Kuznetsova, A., Brockhoff, P. B., & Christensen, R. H. B. (2017). lmerTest Package: Tests in Linear Mixed Effects Models. *Journal of Statistical Software*, *82*, 1–26.

Kybic, J., Clerc, M., Abboud, T., Faugeras, O., Keriven, R., & Papadopoulo, T. (2005). A common formalism for the Integral formulations of the forward EEG problem. *IEEE Transactions on Medical Imaging*, *24*, 12–28.

Lakatos, P., Shah, A. S., Knuth, K. H., Ulbert, I., Karmos, G., & Schroeder, C. E. (2005). An oscillatory hierarchy controlling neuronal excitability and stimulus processing in the auditory cortex. *Journal of neurophysiology*, *94*, 1904–1911.

Lopes da Silva, F. (2004). Functional localization of brain sources using EEG and/or MEG data: volume conductor and source models. *Magnetic resonance imaging*, *22*, 1533–1538.

Morey, R. D. (2008). Confidence Intervals from Normalized Data: A correction to Cousineau (2005). *Tutorial in Quantitative Methods for Psychology*, *4*, 61–64.

Müller, N., Keil, J., Obleser, J., Schulz, H., Grunwald, T., Bernays, R.-L., Huppertz, H.-J., & Weisz, N. (2013). You can't stop the music: reduced auditory alpha power and coupling between auditory and memory regions facilitate the illusory perception of music during noise. *NeuroImage*, *79*, 383–393.

Muthén, B. O. (1998-2004). *Mplus Technical Appendices*. Los Angeles, CA: Muthén & Muthén.

Muthén, L. K., & Muthén, B. O. (1998-2017). *Mplus User´s Guide. Eighth Edition*. Los Angeles, CA: Muthén & Muthén.

Nicholson Peterson, N., Schroeder, C. E., & Arezzo, J. C. (1995). Neural generators of early cortical somatosensory evoked potentials in the awake monkey. *Electroencephalography and Clinical Neurophysiology/Evoked Potentials Section*, *96*, 248–260.

Oldfield, R. C. (1971). The assessment and analysis of handedness: The Edinburgh inventory. *Neuropsychologia*, *9*, 97–113.

Palva, J. M., Zhigalov, A., Hirvonen, J., Korhonen, O., Linkenkaer-Hansen, K., & Palva, S. (2013). Neuronal long-range temporal correlations and avalanche dynamics are correlated with behavioral scaling laws. *Proceedings of the National Academy of Sciences of the United States of America*, *110*, 3585–3590.

Pascual-Marqui, R. D. (2007). Discrete, 3D distributed linear imaging methods of electric neuronal activity. Part 1: exact, zero error localization. *arXiv*.

R Core Team (2018). *R: A language and environment for statistical computing*: R Foundation for Statistical Computing, Vienna, Austria.

Romei, V., Brodbeck, V., Michel, C., Amedi, A., Pascual-Leone, A., & Thut, G. (2008). Spontaneous fluctuations in posterior alpha-band EEG activity reflect variability in excitability of human visual areas. *Cerebral Cortex*, *18*, 2010–2018.

Samaha, J., Iemi, L., Haegens, S., & Busch, N. A. (2020). Spontaneous Brain Oscillations and Perceptual Decision-Making. *Trends in cognitive sciences*, *24*, 639–653.

Samaha, J., Iemi, L., & Postle, B. R. (2017). Prestimulus alpha-band power biases visual discrimination confidence, but not accuracy. *Consciousness and cognition*, *54*, 47–55.

Satterthwaite, F. E. (1946). An Approximate Distribution of Estimates of Variance Components. *Biometrics Bulletin*, *2*, 110.

Stephani, T., Waterstraat, G., Haufe, S., Curio, G., Villringer, A., & Nikulin, V. V. (2020). Temporal Signatures of Criticality in Human Cortical Excitability as Probed by Early Somatosensory Responses. *The Journal of Neuroscience*, *40*, 6572–6583.

Tadel, F., Baillet, S., Mosher, J. C., Pantazis, D., & Leahy, R. M. (2011). Brainstorm: a user-friendly application for MEG/EEG analysis. *Computational intelligence and neuroscience*, *2011*, 879716.

Waterstraat, G., Fedele, T., Burghoff, M., Scheer, H.-J., & Curio, G. (2015). Recording human cortical population spikes non-invasively--An EEG tutorial. *Journal of neuroscience methods*, *250*, 74–84.

Wikström, H., Huttunen, J., Korvenoja, A., Virtanen, J., Salonen, O., Aronen, H., & Ilmoniemi, R. J. (1996). Effects of interstimulus interval on somatosensory evoked magnetic fields (SEFs): A hypothesis concerning SEF generation at the primary sensorimotor cortex. *Electroencephalography and Clinical Neurophysiology/Evoked Potentials Section*, *100*, 479–487.